

Contrast of artificial subcutaneous hematomas in MRI over time

Eva Maria Hassler · Kathrin Ogris · Andreas Petrovic ·
Bernhard Neumayer · Thomas Widek · Kathrin Yen ·
Eva Scheurer

Received: 22 June 2014 / Accepted: 11 November 2014 / Published online: 23 November 2014
© Springer-Verlag Berlin Heidelberg 2014

Abstract In clinical forensic medicine, hematomas and other externally visible injuries build the basis for the reconstruction of events. However, dating of subcutaneous hematomas based on their external aspect is difficult. Magnetic resonance imaging (MRI) has proven its use in dating intracranial hemorrhage. Thus, the aim was to investigate if MRI can also be used for dating subcutaneous hematomas and to analyze an eventual influence of the hematoma shape. In 20 healthy volunteers (11 females, 9 males, aged 26.9 ± 3.8 years), 4 ml of autologous blood were injected subcutaneously in the thigh. The hematoma was scanned immediately after the injection, after 3 and 24 h and 3, 7, and 14 days using three sequences with different contrast. Data was analyzed by measuring signal intensities of the hematoma, the muscle, and the subcutaneous tissue over time, and the Michelson contrast coefficients between the tissues were calculated. In the analysis, hematoma shape was considered. Signal intensity of

blood in the proton density-weighted sequence reached its maximum 3 h after the injection with a subsequent decrease, whereas the signal intensities of muscle and fatty tissue remained constant. The time course of the Michelson coefficient of blood versus muscle decreased exponentially with a change from hyperintensity to hypointensity at 116.9 h, depending on hematoma shape. In the other sequences, either variability was large or contrast coefficients stayed constant over time. The observed change of contrast of blood versus muscle permits a quick estimate of a hematoma's age. The consideration of the hematoma shape is expected to further enhance dating using MRI.

Keywords Dating · Wound age · MRI · Forensic medicine · Subcutaneous tissue · Hematoma

E. M. Hassler · K. Ogris · A. Petrovic · B. Neumayer · T. Widek ·
E. Scheurer (✉)

Ludwig Boltzmann Institute for Clinical Forensic Imaging,
Universitätsplatz 4/II, 8010 Graz, Austria
e-mail: eva.scheurer@bs.ch

E. M. Hassler
Department of Radiology, Division of General Diagnostic
Radiology, Medical University of Graz, Auenbruggerplatz 9,
8036 Graz, Austria

K. Ogris · E. Scheurer
Institute of Forensic Medicine, Medical University Graz,
Universitätsplatz 4/II, 8010 Graz, Austria

A. Petrovic
Institute of Biomedical Engineering, University of Technology Graz,
Kronsgasse 5/II, 8010 Graz, Austria

K. Yen
Institute for Forensic and Traffic Medicine, University of Heidelberg,
Voßstraße 2, 69115 Heidelberg, Germany

Introduction

Clinical radiologists use magnetic resonance imaging (MRI) signal characteristics of intracranial hemorrhage and the corresponding time-dependent changes in their everyday routine since they were first described in the 1980s [1–3]. Since then, the knowledge about the underlying pathophysiological processes which affect the magnetic behavior of blood, like hemostasis, blood clotting, and the changes in the hemoglobin oxygen state, has constantly grown [1, 4–9]. However, in contrast to the numerous studies, which exist about intracranial hemorrhage, only few concentrate on extracranial hematomas. The main reason might be that mostly extracranial hematomas have no diagnostic or therapeutic consequence for patients and, thus, lack importance in clinical research. Radiology literature on soft tissue hemorrhage focuses mainly on the differentiation of bleedings from other soft tissue masses such as tumors [10, 11].

Few authors investigated time-dependent changes of the magnetic properties and relaxation parameters of extracranial hematomas relating to the degradation process of hemoglobin and its breakdown products like deoxyhemoglobin, methemoglobin, and hemosiderin over time using MRI [9, 12, 13]. These studies aimed at an evaluation of the hematoma properties in MRI in order to facilitate detection of hemorrhage in clinical situations. The studies consisted of investigations of artificially created hematomas in animals [9, 12] as well as of accidental hematomas of various ages and in different body regions in patients [9, 13]. Clinical forensic imaging is focused on the forensic analysis of trauma and the reconstruction of events in living victims, e.g., following interpersonal violence, child maltreatment, or sexual abuse. Reliable detection, morphological characterization, and dating of injuries are important and an ongoing issue in forensic research [14, 15]. However, to date, there exists no objective and reliable method for dating subcutaneous bruises which can be used in clinical forensic routine. The current standard is an external inspection with a subjective visual evaluation of the color of the bruise.

On the basis of its successful application in intracranial hemorrhage and the increasing use in forensic medicine, preliminary studies for dating subcutaneous hematomas using MRI were performed, and it was shown that the contrast between blood and muscle and fatty tissue, respectively, might be an indicator for the age of a subcutaneous hemorrhage [16, 17]. As initial results have shown the degradation of blood in soft tissues of living persons also depends on the distribution of the blood in the surrounding tissue and the geometrical shape of the blood volume [13, 18].

Thus, the aim of this study was (a) to systematically analyze contrast of subcutaneous hematomas versus skeletal muscle and versus subcutaneous fat in different MRI sequences and (b) to determine the influence of hematoma shape on the contrast change over time.

Materials and methods

Twenty healthy volunteers (11 females, 9 males, age 26.9 ± 3.8 years (mean \pm SD)) without coagulation disorders or medication influencing blood clotting underwent an initial MRI scan of the thigh which served as a baseline scan of the region of interest in order to plan the depth and the exact location of injection. Ten milliliters of blood were drawn from the cubital vein. Immediately thereafter, 4 ml of this blood were injected into the subcutaneous fatty tissue of the internal anterior side of the thigh, i.e., at the position which had been planned after the baseline scan. The hereby created artificial hematoma was scanned repetitively, i.e., directly after the injection, and at 3 h and 24 h, 3 days, and 1 and 2 weeks after the injection. With the remaining 6 ml, a blood gas analysis was conducted

(hemoglobin concentration, hematocrit, pH, oxygen saturation, fraction of oxyhemoglobin, fraction of deoxyhemoglobin, fraction of methemoglobin). Additionally, a photographic documentation of the external aspect of the hematoma was performed at every examination. The study was approved by the responsible ethics committee located at the local medical university, and written informed consent was obtained from all study participants prior to enrolling in the study.

All MRI measurements were performed on a 3T MRI scanner (Tim Trio, Siemens AG, Erlangen, Germany) using one part of an eight-channel cloth pin coil (Noras MRI products GmbH, Hoechberg, Germany). The protocol consisted of three sequences: (1) proton density-weighted turbo spin echo with SPAIR fat suppression (PDwSPAIR), (2) T1w turbo inversion recovery (TIR) with different inversion times, and (3) multi-echo spin echo (MSE) where the echo at 108 ms was used to obtain T2 weighting. The sequence parameters are listed in Table 1. All sequences were conducted in plane of the artificial hematoma which was oblique with respect to the axes of the thigh; the PDw sequence was additionally performed in transverse orientation. The chosen sequences and weightings are commonly used in standard clinical musculoskeletal imaging. Essentially, they illustrate fluid collection and edema in soft tissue in order to investigate, e.g., intramuscular bleedings or soft tissue inflammation. However, the sequence parameters were especially adapted to achieve good contrast between blood, muscle, and fatty tissue.

Six volunteers were excluded from the data analysis due to technical reasons including severe motion artifacts. Thus, data of 14 volunteers (6 females, 8 males, age 26.9 ± 3.9 years) were analyzed by a forensic researcher on a post-processing workstation (MMWP, Siemens AG, Erlangen, Germany). All three sequences, PDwSPAIR (in oblique orientation as for the other sequences), TIR, and MSE, of all six examinations after injection were used for analysis.

Three circular ROIs (size, $0.40\text{--}0.55\text{ cm}^2$) were placed each in the hematoma, in the underlying muscle tissue, and in the surrounding subcutaneous fatty tissue for the measurement of signal intensity (SI). Figure 1 illustrates the placement of the ROIs. The three measurements per tissue were averaged for further analysis. For each of the examination times, contrast coefficients according to Michelson [19] ($C_M = (SI_1 - SI_2) / (SI_1 + SI_2)$) were calculated for the contrast between blood and fatty tissue and between blood and muscle tissue, respectively, using Matlab (2011b, TheMathworks Inc, Natick, MA, USA). It was investigated if the time course of the Michelson coefficient could be described by an unequivocal mathematical function.

Additionally, a visual evaluation of the shape of the hematomas and the lobular structure of the subcutaneous fatty tissue was performed. The result of this visual assessment was taken into account as an additional factor for the

Table 1 Acquisition parameters of the used MR sequences

Sequence	FOV (mm)	Readout matrix	Slice thickness (mm)	TR (ms)	TE (ms)	TI (ms)	Acquisition time (min)
PDwSPAIR	100	192	1.5	3400	11	–	03:39
TIR	100	192	1.5	7000	11	200	02:50
MSE (T2w)	100	192	1.5	5000	108	–	14:52

mathematical modeling of the Michelson coefficient in PDwSPAIR images over time in order to evaluate an eventual effect of the shape.

Results

Figure 2 shows a representative example of an artificial hematoma in all evaluated sequences and demonstrates good image quality. In all sequences, the SI of the fatty tissue and the muscle tissue remained relatively constant during the entire observation period, while the SI of the hematoma blood shows different time courses in the three sequences.

In the PDwSPAIR sequence, the SI of the hematoma was highly positive in comparison to the other tissues at the beginning of the measurements, and then subsequently decreased during the 2 weeks of examination. The difference of SI between blood and fatty tissue decreased over time (from 122.8–433.1 at the beginning to 37.0–230.5 after 7 days), but the hyperintensity of the hematoma versus fat is still well visible after 1 week. In the TIR sequence, the hematoma showed a negative contrast behavior versus muscle and fatty tissue, respectively, and after 7 days, the hematoma could scarcely be differentiated from the surrounding fatty tissue. In the MSE sequence, the hematoma was hypointense versus fatty tissue, and SI increased over time when averaged over all volunteers to reach almost the same SI as the subcutaneous fat after 2 weeks. Compared to muscle tissue, the artificial

hematomas showed very high SI at the beginning, and with increasing time, the SI further increased while the SI of skeletal muscle was constant. The measured SI values for all volunteers are shown in detail in Table 2, whereas Table 3 gives a comprehensive overview on median and range of SI values directly post-injection and after 2 weeks. A qualitative description of the contrast of the artificial subcutaneous hematomas versus the surrounding tissues in the three sequences over time is given in Table 4.

Figure 3 shows the time course of the Michelson contrast coefficients of blood versus fatty tissue in the different sequences. The PDwSPAIR sequence yielded the highest contrast between hematoma blood and fatty tissue with a Michelson coefficient of 0.83 ± 0.04 (mean \pm SD) directly after the injection and a value of 0.51 ± 0.10 after 2 weeks. The hematoma was hyperintense compared to the fatty tissue during the whole period of observation. In TIR (Fig. 3b), the contrast coefficient was negative and increased during the entire examination period from -0.55 ± 0.11 on the first day to -0.16 ± 0.08 at the last measurement. The Michelson coefficient of blood versus fat showed a similar variability as in the PDwSPAIR with standard deviations of 0.04 to 0.10. In the MSE sequence, the Michelson coefficient showed the largest variability without a characteristic curve progression. At the beginning, the variability was lowest in PDwSPAIR, whereas

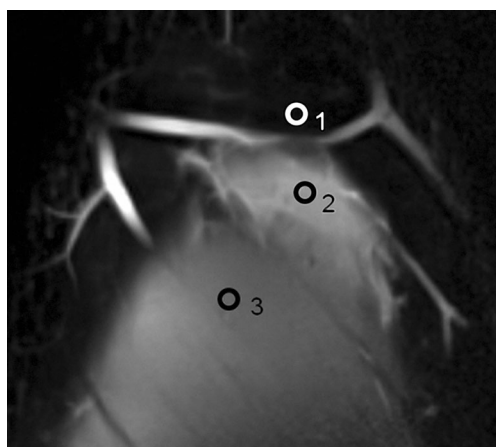


Fig. 1 PDwSPAIR image in oblique orientation showing the placement of the ROIs in the three different tissues (1 fatty tissue, 2 hematoma, 3 muscle tissue)

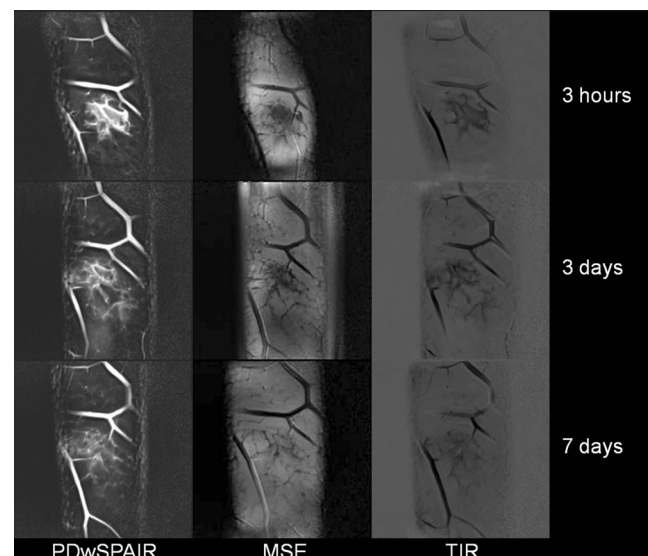


Fig. 2 MR images of an artificial hematoma at different time points in the three evaluated sequences (PDwSPAIR, TIR, MSE) in oblique orientation through the subcutaneous fatty tissue of the thigh

Table 2 Shows all SI measurements of the volunteers

Volunteer	Sex	Sequence	SI	SI	SI	SI	SI	SI muscle	SI
			3 h	24 h	3 days	7 days	14 days	s.c. fat	
1	M	PDwSPAIR	216.6	273.1	150.5	116.3	79.3	122.1	21.2
		T1w TIR	-162.8	-280.1	-153.7	-87.6	-69.5	-62.3	-57.1
		T2w MSE	152.8	199.2	187.4	255.0	205.7	21.4	463.0
2	F	PDwSPAIR	249.3	185.7	105.5	67.3	37.0	92.6	19.8
		T1w TIR	-218.8	-171.6	-124.5	-87.2	-50.2	-53.3	-52.2
		T2w MSE	244.6	219.9	148.3	178.0	185.4	13.2	275.2
3	M	PDwSPAIR	278.2	268.8	188.5	164.8	106.1	165.5	26.5
		T1w TIR	-256.3	-243.7	-156.0	-135.2	-89.8	-77.5	-60.9
		T2w MSE	190.8	164.2	143.3	234.3	227.3	24.6	354.3
4	F	PDwSPAIR	201.5	220.0	146.9	138.0	108.5	155.1	21.6
		T1w TIR	-178.1	-198.2	-170.4	-146.1	-114.0	-92.2	-80.9
		T2w MSE	166.3	225.2	230.4	269.0	308.5	25.0	444.9
5	F	PDwSPAIR	222.4	307.7	187.3	136.6	63.2	133.7	23.8
		T1w TIR	-261.4	-252.5	-222.3	-147.0	-100.4	-70.4	-69.8
		T2w MSE	236.9	326.8	319.7	369.5	366.0	23.3	422.8
6	M	PDwSPAIR	233.9	262.9	198.8	129.1	84.4	163.0	23.2
		T1w TIR	-254.9	-258.1	-253.5	-148.9	-122.3	-85.0	-78.0
		T2w MSE	245.5	328.7	353.8	335.1	329.7	20.9	452.0
7	M	PDwSPAIR	316.2	332.7	295.6	181.3	174.5	173.3	39.1
		T1w TIR	-248.6	-295.1	-239.8	-140.8	-139.9	-89.9	-64.7
		T2w MSE	134.5	215.4	181.0	148.8	265.5	23.3	362.7
8	F	PDwSPAIR	285.3	199.4	188.7	102.7	65.1	167.0	20.0
		T1w TIR	-312.4	-238.5	-195.9	-136.6	-99.4	-86.1	-71.0
		T2w MSE	387.6	496.2	466.1	382.7	377.0	27.6	546.7
9	F	PDwSPAIR	271.5	176.7	134.0	97.3	NA	116.6	15.5
		T1w TIR	-265.9	-159.1	-135.4	-108.1	NA	-67.8	-52.3
		T2w MSE	235.4	258.5	340.4	344.3	NA	18.8	332.8
10	M	PDwSPAIR	163.6	171.6	146.8	79.7	50.2	124.4	23.9
		T1w TIR	-150.2	-171.5	-136.2	-103.9	-70.7	-65.1	-59.5
		T2w MSE	140.0	184.7	206.7	231.5	253.0	18.4	329.6
11	M	PDwSPAIR	275.0	325.1	227.4	166.1	97.0	210.2	36.2
		T1w TIR	-223.7	-234.1	-214.8	-174.9	-101.0	-98.3	-67.4
		T2w MSE	225.9	313.0	310.7	287.5	427.1	25.1	444.8
12	F	PDwSPAIR	198.0	211.4	160.8	110.1	79.8	132.6	30.8
		T1w TIR	-176.3	-172.5	-148.5	-128.9	-91.1	-70.3	-58.9
		T2w MSE	145.9	162.4	204.7	243.5	212.7	19.2	363.4
13	M	PDwSPAIR	402.0	269.9	218.4	116.3	79.4	181.0	32.3
		T1w TIR	-270.3	-276.2	-179.0	-210.1	-135.2	-91.4	-95.3
		T2w MSE	461.5	512.4	359.6	503.6	564.0	27.5	539.2
14	M	PDwSPAIR	311.6	209.1	197.8	132.1	82.0	165.1	27.2
		T1w TIR	-272.9	-210.6	-209.2	-132.9	-88.0	-86.9	-71.4
		T2w MSE	165.3	282.2	300.7	240.3	312.8	28.1	502.0

in MSE, the contrast coefficients showed the largest variability over the entire investigation period (0.15–0.23).

The time course of the Michelson contrast coefficient of blood versus muscle tissue is shown in Fig. 4. In the PDwSPAIR sequence, the contrast coefficient with an initial

value of 0.30 ± 0.07 steadily decreased and became negative between measurement 4 on day 3 and measurement 5 after 1 week to reach a minimum of -0.34 ± 0.06 after 2 weeks. For the TIR sequence, also an increase was observed over the 2 weeks, i.e., from -0.55 ± 0.07 to -0.11 ± 0.07 . In the MSE

Table 3 Median and range of signal intensity values in all evaluated sequences directly post injection (P.I.) and after an investigation period of 2 weeks

	P.I.	After 2 weeks
PDwSPAIR		
Hematoma	291.6 (122.8 to 433.1)	79.8 (37.0 to 230.5)
Muscle	47.2 (17.2 to 196.1)	26.7 (9.8 to 141.9)
Fatty tissue	25.1 (9.1 to 30.8)	28.3 (17.3 to 48.1)
TIR		
Hematoma	-251.1 (-383.7 to -92.3)	-99.4 (-225.9 to -50.0)
Muscle	-80.6 (-142.3 to -71.0)	-76.0 (-180.6 to -49.9)
Fatty tissue	-66.9 (-105.5 to 21.9)	-60.9 (-90.9 to 3.0)
MSE		
Hematoma	192.5 (111.9 to 419.2)	306.3 (164.2 to 564.0)
Muscle	22.9 (14.1 to 60.8)	22.6 (12.1 to 62.9)
Fatty tissue	405.2 (237.0 to 634.3)	455.85 (213.6 to 613.3)

sequence, the contrast coefficient stayed relatively constant over the entire investigation period and showed large variability compared to the small dynamic range.

The decrease of the Michelson coefficients between blood and muscle in PDwSPAIR could be described by the mono-exponential function $C_M = 0.77 \exp(-t/245) - 0.48$, which crosses the zero baseline at 116.9 h after injection, changing from a positive Michelson coefficient blood/muscle to negative values afterwards (Fig. 5a).

Visual analysis of the hematomas resulted in a classification of two categories of hematoma shapes depending on the surrounding fatty tissue (a) showing a compact volume and (b) with a diffuse distribution in the subcutaneous tissue (see examples in Fig. 6). In the compact hematoma type, the blood volume appeared as a compact accumulation of blood with a rather smooth circumference surrounded by fusiform-shaped fat lobules, while in the diffuse hematoma type, the blood entered into the clefts between the fatty lobules which were spherically shaped. A classification of all hematomas was

Table 4 Qualitative description of the signal behavior of the artificial hematoma versus the surrounding tissues in the three evaluated sequences

	Acute	1 day	3 days	1 week	2 weeks
Hematoma vs. muscle					
PDwSPAIR	+	+	+	-	-
TIR	-	-	-	-	=
MSE	+	+	+	+	+
Hematoma vs. fatty tissue					
PDwSPAIR	+	+	+	+	+
TIR	-	-	-	-	-/=
MSE	-	-	-	-/=	=

- stands for hypointense, + stands for hyperintense, = stands for isointense

possible resulting in a group of eight categorized as compact type and a group of six hematomas classified as diffuse type. By considering this classification, two different times for the transition from positive to negative contrast of the blood versus muscle were found in PDwSPAIR, which was at 133.2 h for the compact type and at 98.8 h for the diffuse type (Fig. 5b).

Discussion

In view of a potential future use for the assessment of the hematoma age in clinical forensic medicine, the contrast changes of artificially created hematomas were measured repetitively over a period of 2 weeks using MRI to evaluate the time course of the contrast of the hemorrhage versus the surrounding tissues in different MRI sequences and to assess potential differences caused by the hematoma shape.

The current standard regarding age estimation of hematomas is an external inspection and visual evaluation of the color of the bruise, although prior studies have shown that the external aspect of subcutaneous bleedings is not reliable as the sequence of colors varies and, additionally, the visible color depends on multiple factors, e.g., the person's age, skin thickness, and skin pigmentation as well as the concerned body region [20, 21]. It has been shown that solely the yellow component could serve as an indicator for non-recent hematomas. However, the perception of the color yellow also varies individually and changes with the age of the examiner [22, 23]. In order to find a more objective and reliable alternative, reflectance spectroscopy was investigated [24]. Using an analytical model to describe the blood distribution in bruised skin as a function of time after injury, the age of bruises could be determined with an accuracy of approximately 1 day. However, the accuracy depends on precise information of skin thickness and is also influenced by the location of the bruise on the body, i.e., if the area is plane or curved. In a study using MRI for the investigation of soft tissue hematomas, Spielmann et al. visually assessed signal intensity (SI) of the hematoma versus muscle in acute hemorrhage up to 3 h at 1.5 T [13] and concluded that signal intensity in fresh hemorrhage could be high or low in T2-weighted images depending on the distribution and oxygen saturation of the erythrocytes as well as on the surrounding tissue, i.e., the location of the hematoma, and, additionally, on the used field strength. In differently aged hematomas, they found that SI changed compared to that of skeletal muscle from isointense to hyperintense in T1-weighted images and from hyper- or hypointense to hypointense in the acute stage, followed again by hyperintensity in the subacute phase, i.e., after some weeks.

In this study, characteristic changes of signal intensity of the injected blood over time were observed in all three evaluated sequences, whereas the values of muscle and fatty tissue

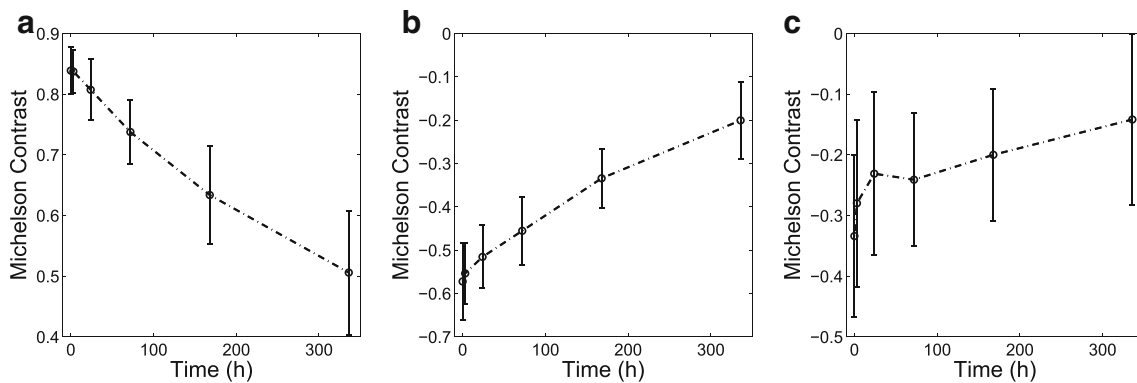


Fig. 3 Time course of the Michelson contrast coefficient (mean and SD) of blood versus subcutaneous fatty tissue in the **a** PDwSPAIR, **b** TIR, and **c** MSE sequence

stayed relatively constant. Immediately after injection, the signal of the hematoma was substantially different from that of muscle and fat in all sequences. Subsequently, during the examination period of 2 weeks, the hematoma signal changed and approached that of fatty tissue due to the degradation of the blood.

The observed MRI signal behavior can be partly explained based on the descriptions of MRI changes in intracranial hemorrhage, where a shortening of the T2 relaxation time associated with the process of deoxygenation of the extravasated blood has been observed [4, 11]. The following methemoglobin formation was described to result in T1 shortening, while later, cell lysis leads to an increase of T2 again [7]. These known changes of relaxation parameters could be a reason for the observed signal increase in the T2-weighted MSE and the TIR, which can be explained by T1 shortening due to methemoglobin formation. However, the acute loss of signal in T2-weighted images based on deoxygenation of the hemoglobin as described in the literature was not observed in this study [11, 13, 10]. An explanation is offered by Spielmann et al. who compared intramuscular to subcutaneous hematomas and found that in hemorrhage localized in gaps between tissues as well as in the subcutaneous fat, high signal intensity can persist due to the counteracting of the tight packing of erythrocytes in the blood clot [12]. Additionally, in

subcutaneous tissue, an important factor influencing signal behavior after some days is the degradation and resorption of the blood. This can be observed in the PDw sequence where T1 and T2 effects are negligible, and the signal of the hematoma approaches that of the fatty tissue with increasing time. This assumption could be confirmed by preliminary results of a quantitative analysis of MRI data using fat-water separation of degrading hematomas [25].

The contrast of injected blood versus surrounding tissues expressed as Michelson coefficient showed characteristic time courses in the three sequences. In the T2-weighted sequence (MSE), contrast changed only slightly, and measurements showed a great variability, indicating low reproducibility and limited potential for hematoma dating. In contrast, changes of hematoma contrast in TIR and PDw sequences were highly reproducible with an unequivocal and steady time course over a period of 2 weeks and reasonable variability. Due to its large dynamic range over time, the contrast of blood versus muscle observed in the PD-weighted sequence suits best for an evaluation of a hematoma's age. The decrease of the contrast over time could be described mathematically by a mono-exponential function, which in the future can be the basis for building a quantitative model for hematoma dating. Additionally, the transition of the contrast of blood versus muscle from hyper-

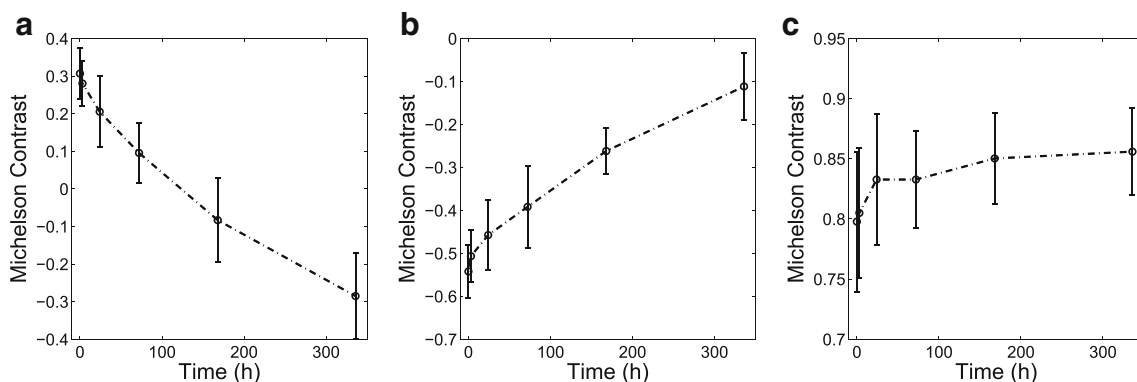
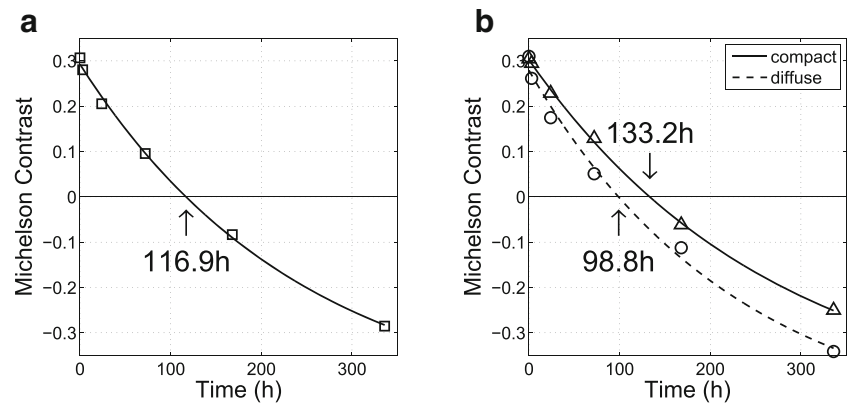


Fig. 4 Time course of the Michelson contrast coefficient (mean and SD) of blood versus muscle tissue in the **a** PDwSPAIR, **b** TIR, and **c** MSE sequence

Fig. 5 Mono-exponential fit of the time course of the Michelson contrast coefficient of blood versus muscle tissue over 2 weeks. **a** Whole averaged data with a baseline crossing at 116.9 h (arrow) and **b** averaged data separated into the two groups of hematoma type: compact and diffuse



hypointensity after about 5 days allows for a quick classification of a hematoma into younger or older than 5 days without any calculation.

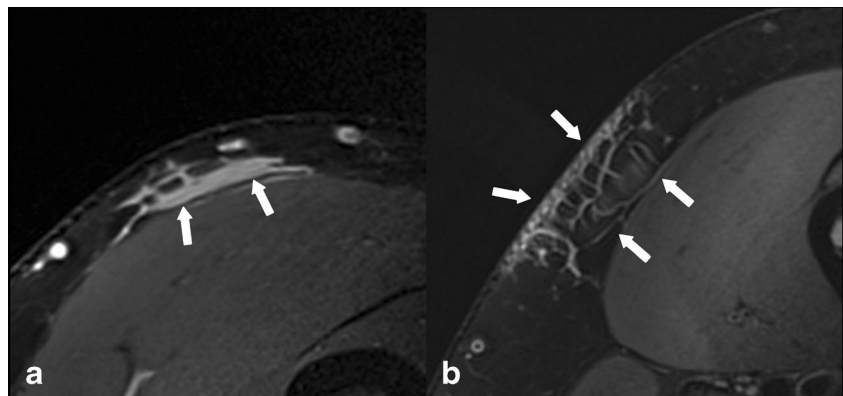
The general tendency found in the literature dealing with extracranial hematomas is that their appearance is usually more complex and inhomogeneous than intracranial hematoma [10, 26] and that the time scale of signal changes shows no linear but a more gradual progression [11, 27, 28]. Also the localization (muscle, fatty tissue) influences the signal alterations as shown by Spielmann et al. in an experimental animal study [12].

Besides these known factors, it was observed here that the shape of the hematoma and morphology of the surrounding fatty lobules leads to a difference in signal change over time. The differentiation between compact and diffuse hematomas resulted in a different time course of contrast and, consequently, in a time difference for the transition from hyper- to hypointensity in the PD-weighted sequence. The diffuse type showed a more rapid decrease of the contrast of blood versus muscle. This is most probably caused by the larger surface and the broader distribution of the blood between the lobules of the fatty tissue which enhances resorption and, thus, accelerates the degradation process. As the time difference for the transition from hyper- to hypointensity between the two types is almost 1.5 days, it is important to consider the shape of the hematoma for an estimation of the time of origin. However, a

more detailed evaluation including the potential influence of sex or body mass and composition on the shape of the hematoma and on hematoma resorption must be based on a larger cohort.

One factor causing variability in MRI is inhomogeneous coil sensitivities. To circumvent this issue, the Michelson contrast coefficient was used for data analysis which allows for a comparison of different subjects by measuring the relation between the spread and the sum of two signal intensities. Thereby, it is possible to generate contrast values independent of signal variation due to inhomogeneous coil sensitivity. An important limitation of this study is that the examined hematomas were artificial and originated from injected blood and do not correspond to real bruises which include a contusional component. Nonetheless, the results of this study which describe the signal behavior of a certain amount of blood during degradation and resorption can be the first step prior to including additional factors such as contusion. Together with a validation of the presented results by examining a greater study cohort and by investigating traumatic bruises of the subcutaneous tissue, the optimization of applied MRI sequences, e.g., using the specific relaxation times of the different tissues, might further enhance the characterization of subcutaneous hemorrhage. The intended application of MRI for an observer independent estimation of hematoma age in clinical forensic medicine has the advantage of allowing on

Fig. 6 Examples of the aspect of the two types of hematoma shape in the subcutaneous fatty tissue (PDwSPAIR axial images at the level of the distal femur): **a** compact hematoma surrounded by fusiform shaped fat lobuli and **b** diffuse hematoma surrounded by spherical fat lobuli (indicated by arrows)



one hand a quick visual assessment and on the other hand the use of a mathematical model incorporating different factors and parameters based on quantitative data of a specific hematoma finding. The current way of hematoma age estimation in the course of an external examination can thus be optimally supplemented in case accurate dating is needed.

To conclude, it was found that the proton density-weighted sequence is especially useful for hematoma dating. The time course of the contrast of blood versus muscle over 2 weeks showed a decreasing mono-exponential function, which can be used to build a model for objective dating of subcutaneous hematomas. The transition of the hematoma contrast from hyper- to hypointense allows for a quick classification of the age of the hematoma into younger and older than about 5 days. Further improvement is possible when taking into account the surrounding tissue by classifying the shape of the hematoma into diffuse or compact, respectively. As the highest contrast between hematoma and surrounding tissue was observed within the first 24 h MRI for the detection and dating of hematomas should be performed as soon as possible after their traumatic origin.

References

- Gomori JM, Grossman RI, Goldberg HI, Zimmerman RA, Bilaniuk LT (1985) Intracranial hematomas: imaging by high-field MR. *Radiology* 157(1):87–93
- Zyed A, Hayman LA, Bryan RN (1991) MR imaging of intracerebral blood: diversity in the temporal pattern at 0.5 and 1.0 T. *AJNR Am J Neuroradiol* 12(3):469–474
- Hayman LA, McArdle CB, Taber KH, Saleem A, Baskin D, Lee HS, Kirkpatrick JB, Herrick RC, Bryan RN (1989) MR imaging of hyperacute intracranial hemorrhage in the cat. *AJNR Am J Neuroradiol* 10(4):681–686
- Bradley WG Jr (1993) MR appearance of hemorrhage in the brain. *Radiology* 189(1):15–26
- Hayman LA, Taber KH, Ford JJ, Bryan RN (1991) Mechanisms of MR signal alteration by acute intracerebral blood: old concepts and new theories. *AJNR Am J Neuroradiol* 12(5):899–907
- Allkemper T, Tombach B, Schwindt W, Kugel H, Schilling M, Debus O, Mollmann F, Heindel W (2004) Acute and subacute intracerebral hemorrhages: comparison of MR imaging at 1.5 and 3.0 T—initial experience. *Radiology* 232(3):874–881. doi:10.1148/radiol.2323030322
- Bradley WGJ, Schmidt PG (1985) Effect of methemoglobin formation on the MR appearance of subarachnoid hemorrhage. *Radiology* 156(1):99–103
- Hayman LA, Taber KH, Ford JJ, Saleem A, Gurgun M, Mohamed S, Bryan RN (1989) Effect of clot formation and retraction on spin-echo MR images of blood: an in vitro study. *AJNR Am J Neuroradiol* 10(6):1155–1158
- Swensen SJ, Keller PL, Berquist TH, McLeod RA, Stephens DH (1985) Magnetic resonance imaging of hemorrhage. *AJR Am J Roentgenol* 145(5):921–927
- Bush CH (2000) The magnetic resonance imaging of musculoskeletal hemorrhage. *Skelet Radiol* 29(1):1–9
- Rubin JI, Gomori JM, Grossman RI, Gefter WB, Kressel HY (1987) High-field MR imaging of extracranial hematomas. *AJR Am J Roentgenol* 148(4):813–817
- Spielmann RP, Maas R, Neumann C, Dallek M, Nicolas V, Heller M, Bucheler E (1990) MRT of acute soft tissue hematomas at 1.5 T: animal experimental results. *Röfo* 153(4):395–399. doi:10.1055/s-2008-1033402
- Spielmann RP, Triebel HJ, Maas R, Langkowski J, Franz P, Heller M, Bucheler E (1989) MRT of extracranial hematomas at 1.5 T using spin echo and gradient echo sequences. *Röfo* 150(4):449–453. doi:10.1055/s-2008-1047054
- Malli N, Ehammer T, Yen K, Scheurer E (2013) Detection and characterization of traumatic scalp injuries for forensic evaluation using computed tomography. *Int J Legal Med* 127(1):195–200. doi:10.1007/s00414-012-0690-x
- Yen K, Vock P, Tiefenthaler B, Ranner G, Scheurer E, Thali MJ, Zwygart K, Sonnenschein M, Wiltgen M, Dirnhofner R (2004) Virtopsy: forensic traumatology of the subcutaneous fatty tissue; multislice computed tomography (MSCT) and magnetic resonance imaging (MRI) as diagnostic tools. *J Forensic Sci* 49(4):799–806
- Neumayer B, Hassler E, Widek T, Petrovic A, Scheurer E (2012) Modelling of contrast changes in soft tissue hematomas. 29th Annual Meeting ESMRMB, Lisbon, pp 4–6
- Hassler E, Neumayer B, Petrovic A, Ogris K, Widek T, Yen K, Scheurer E (2012) Contrast evaluation of artificial hematomas in different MRI sequences over time. 29th Annual Meeting ESMRMB, Lisbon, pp 4–6
- Ogris K, Hassler EM, Petrovic A, Neumayer B, Widek T, Scheurer E (2014) Evaluation of impact factors in the regeneration process of hematomas in the subcutaneous fatty tissue. Joint Annual Meeting of the ISMRM and ESMRMB, Milan, pp 10–16
- Michelson A (1927) *Studies in optics*. U. of Chicago Press, Chicago
- Pilling ML, Vanezis P, Perrett D, Johnston A (2010) Visual assessment of the timing of bruising by forensic experts. *J Forensic Legal Med* 17(3):143–149. doi:10.1016/j.jflm.2009.10.002
- Langlois NE, Gresham GA (1991) The ageing of bruises: a review and study of the colour changes with time. *Forensic Sci Int* 50(2):227–238
- Hughes VK, Ellis PS, Langlois NE (2004) The perception of yellow in bruises. *J Clin Forensic Med* 11(5):257–259. doi:10.1016/j.jcfm.2004.01.007
- Stephenson T, Bialas Y (1996) Estimation of the age of bruising. *Arch Dis Child* 74(1):53–55
- Randeberg LL, Haugen OA, Haaverstad R, Svaasand LO (2006) A novel approach to age determination of traumatic injuries by reflectance spectroscopy. *Lasers Surg Med* 38(4):277–289. doi:10.1002/lsm.20301
- Petrovic A, Diwoy C, Hassler E, Ogris K, Scheurer E (2013) IDEAL fat-water separation for the detection and characterization of subcutaneous hemorrhage. 21st Annual Meeting ISMRM, Salt Lake City
- Chu B, Kampschulte A, Ferguson MS, Kerwin WS, Yamykh VL, O'Brien KD, Polissar NL, Hatsukami TS, Yuan C (2004) Hemorrhage in the atherosclerotic carotid plaque: a high-resolution MRI study. *Stroke* 35(5):1079–1084. doi:10.1161/01.STR.0000125856.25309.86
- Unger EC, Glazer HS, Lee JK, Ling D (1986) MRI of extracranial hematomas: preliminary observations. *AJR Am J Roentgenol* 146(2):403–407
- Yamashita Y, Hatanaka Y, Torashima M, Takahashi M (1995) Magnetic resonance characteristics of intrapelvic haematomas. *Br J Radiol* 68(813):979–985